Dalton Transactions

A new microporous 12-ring zincosilicate THK-2 with many terminal silanols characterized by automated electron diffraction tomography

Journal:	*Dalton Transactions*
Manuscript ID	DT-ART-06-2020-002290.R1
Article Type:	Paper
Date Submitted by the Author:	24-Aug-2020
Complete List of Authors:	Sakamoto, Yasuhiro; Tohoku University - Katahira Campus, Institute of Multidisciplinary Research for Advanced Materials Zhao, Haishuang; Johannes Gutenberg University Mainz, Institute of Inorganic Chemistry and Analytical Chemistry Gies, Hermann; Ruhr-Universitat-Bochum, Institut fuer Geologie, Mineralogie und Geophysik Yamamoto, Katsutoshi; The University of Kitakyushu, Faculty of Envionmental Engineering Kolb, Ute; Johannes Gutenberg-University, Institut for Physical Chemistry Ikeda, Takuji; National Institute of Advanced Industrial Science and Technology, Research Institute for Chemical Process Technology

A new microporous 12-ring zincosilicate THK-2 with many terminal silanols characterized by automated electron diffraction tomography

Yasuhiro Sakamoto[1,2], Haishuang Zhao[3], Hermann Gies[4], Katsutoshi Yamamoto[5], Ute Kolb[3,*], and Takuji Ikeda[6,*]

[1]*Department of Physical Science, Graduate School of Science, Osaka Prefecture University, 1-1 Gakuen-cho, Naka-ku, Sakai, 599-8531, Japan*

[2]*PRESTO, Japan Science and Technology Agency (JST), 4-1-8 Honcho, Kawaguchi, 332-0012, Japan*

[3]*Institute of Inorganic Chemistry and Analytical Chemistry*, *Duesbergweg 10–14, Johannes Gutenberg-University Mainz*, *55128 Mainz*, *Germany*

[4]*Institute for Geology, Mineralogy and Geophysics, Ruhr-University Bochum 44780 Bochum*, *Germany*

[5]*Faculty of Environmental Engineering*, *The University of Kitakyushu 1-1 Hibikino*, *Wakamatsu-ku*, *Kitakyushu 808-0135*, *Japan*

[6]*Research Institute for Chemical Process Technology*, *National Institute of Advanced Industrial Science and Technology (AIST)*, *4-2-1 Nigatake, Sendai, 983-8551*, *Japan*

[*]Corresponding authors: Takuji Ikeda (T.I), Ute Kolb (U.K)

E-mail: takuji-ikeda@aist.go.jp (T.I), kolb@uni-mainz.de (U.K)

Abstract

The newly synthesized microporous zincosilicate THK-2 (estimated structural composition: $|(H_2O)_{6.7}(C_6H_{13}N)_{0.9}|[Li_{0.5}Zn_{3.1}Si_{32}O_{62.7}(OH)_{9.3}]$) was characterized by single-crystal electron diffraction using automated electron diffraction tomography (ADT) approach in combination with the powder X-ray diffraction. The lattice constants and space group of as-synthesized THK-2 were a = 2.50377(7) nm, b = 1.43866(4) nm, c = 0.505369(8) nm, and *Pccn* (No. 56) belonging to orthorhombic symmetry. Because the crystal lattice is almost identical with a hexagonal lattice (a/b = 1.74 ≈ 1.732), the first several peaks in its powder X-ray diffraction data severely overlapped, which suppresses structural information to decide the framework topology. In order to overcome this intrinsic difficulty, the structure model of THK-2 was initially obtained from the direct method based on ADT data and refined by the Rietveld method. Its 3-dimensional framework structure was elucidated to consist of 4-, 5-, 6-rings of tetrahedral Si and Zn atoms and to have a one-dimensional straight channel with 12-ring pore opening. Zn atoms were incorporated in the framework as four-coordinated [ZnO_4], although its distribution was confirmed to be disorderly. In the as-synthesized THK-2, the site occupancy of Zn was as low as 0.39; that is, more than 60 % of the Zn site was vacant. Hexamethyleneimine and water molecules are disorderly accommodated in the straight channel. The material was stable upon calcination, and the BET specific surface area and micropore volume of calcined THK-2 were 240.6 m^2/g and 0.12 ml/g, respectively.

1. Introduction

Synthetic zeolites, which have well-ordered nanoporous framework structures with, e.g., silicate, aluminosilicate, or aluminophosphate compositions, are among the most critical

materials for various industrial applications such as sorption, separation, ion-exchange, catalysis in petrochemical processes, etc. Among them, heteroatom-substituted zeolites with the possibility as high-performance catalysts attract many researchers, so various heteroatoms such as B, Ga, Ti, Fe, Co, and other transition metal atoms have been substituted for Si atoms in zeolite frameworks to date. In many cases, a small number of heteroatoms can be substituted for a T-atom in the framework structure by hydrothermal synthesis or post-synthesis treatments [1,2]. For example, a titanosilicate TS-1 is well known as a Ti-containing **MFI**-type zeolite, which has been introduced as a catalyst for the conversion from cyclohexanone to cyclohexanone oxime in industrial processes.

The catalytic activity of Zn-modified zeolites for small alkane aromatization has been studied for about three decades [1,2]. In general, Zn-modified zeolites can be prepared by ion-exchange or impregnation of the NH_4^+- or H^+-form of a zeolite with an aqueous solution a zinc salt. For example, it was reported that the Zn-modified ZSM-5 catalyst made in this way demonstrated higher selectivity for aromatics compared to the catalysts based on pure H^+-ZSM-5 zeolite [3,4]. However, Zn substitution for T-sites in the framework may have the advantage for several reasons: (i) Zn on T-sites will not be easily removed from the framework compared with general "non-framework cations." (ii) improvement of catalytic activity. (iii) the effect of micropore blockage will be reduced compared to Zn cations located at the pore opening. Zinc substitution into the frameworks of zeolite LTA or FAU via hydrothermal synthesis has been claimed in a U.S. patent in 1982 [5], although the patent does not show clear experimental evidence that Zn is contained on T-sites in the framework.

For the above reasons, the substitution of Zn for T-sites in zeolite frameworks has been studied for more than a quarter of a century. Among the 248 types of zeolite frameworks known

so far, there are 37 types that include Zn in the framework structure. Furthermore, some of them have been approved as unique zeolite structures, e.g., ZnAlPO-57 (**AFV**) [6], ZnAlPO-59 (**AVL**) [6], Chiral Zincophosphate (**CZP**) [7], RUB-17 (**RSN**) [8], UCSB-10GaZn (**SBT**) [9], VPI-9 (**VNI**) [10], VPI-7 (**VSV**) [11] and ZAPO-M1 (**ZON**) [12]. These zeolites can be obtained by direct hydrothermal synthesis, and the Zn position in framework structure is strictly ordered on symmetrically distinct sites. Their framework structures are known to have unique structural units that are not observed in previously known zeolites, such as spiro-5 subunits centered on Zn atoms observed in **VSV** and **RSN.** Therefore, due to the specificity of the local structure around those Zn atoms, it is sometimes difficult to determine their crystal structures, as is the case with typical zeolites consisting only of TO_4 units. Determining the structure of zeolites by direct methods using powder diffraction data with poor structural information is usually difficult, which makes it more difficult to determine the existence of unique structural units.

Electron crystallography, including imaging and diffraction methods, has been applied successfully to characterize complex structural features in nanocrystalline materials. Electron beam damage as one of the significant problems is significantly reduced using electron diffraction (ED). Automated electron diffraction tomography (ADT) [13–15], developed ten years ago, allows for the collection and analysis of three-dimensional (3D) single-crystal ED data from a single nanosized crystal. This technique differs from the powder X-ray diffraction (XRD), providing only a projection from 3D reciprocal space into one-dimensional data from the overall sample. Hence, the single-crystal ED shows its distinct advantage for the structural investigation of nanocrystalline multiphasic samples [16,17]. For a better understanding and elucidating all structural features, electron diffraction tomography can be used in combination

with other methods such as high resolution transmission electron microscopy (HRTEM) and powder XRD.

In this study, we report the structural characterization of a new nanoporous zincosilicate THK-2. THK-2 was synthesized hydrothermally based on a SiO_2-ZnO-KOH-LiOH-hexamethyleneimine (HMI)-H_2O system. The crystal structure of THK-2 was solved utilizing ADT, the state-of-the-art technology in crystallography. The silicate framework has a one-dimensional 12-ring nano-channel and statically disordered Zn atom distribution on T-sites.

2. Experimental

2.1. Synthesis of THK-2

THK-2 was synthesized in the following manner: lithium hydroxide monohydrate (Kanto Chemical) and potassium hydroxide (Wako Pure Chemical) were dissolved in deionized water under stirring conditions. Zinc acetate dihydrate (Wako Pure Chemical) was added to this solution, and then a white suspension was obtained. Colloidal silica Snowtex-N (Nissan Chemical) and subsequently hexamethyleneimine (HMI, Tokyo Chemical) were added to this suspension, and after 10-minute stirring the, mother gel was obtained. The typical gel composition was SiO_2 : 0.067 ZnO : 0.18 LiOH : 0.18 KOH : 0.5 HMI : 60 H_2O. The mother gel was transferred into a Teflon-lined stainless-steel autoclave and hydrothermally treated at 423 K for 14 days under stirring conditions. The solid product was treated with 50 wt% acetic acid at 333 K to remove impurities, recovered by filtration, washed with deionized water, and dried at room temperature overnight to obtain (as-synthesized) THK-2. The as-synthesized sample was further washed thrice with 1 mM HCl aqueous solution for 1 h at room temperature, and then the sample was calcined at 813 K for 6 h (designated as cal-THK-2) to remove HMI

template molecules.

2.2. Data collection for ADT

The sample (cal-THK-2) was firstly dispersed in ethanol and transferred into a caved tip with a pipette. The specimen dispersion after ultrasonication was sprayed onto a standard Cu microgrid (300 mesh) with a thin amorphous carbon film. HRTEM, scanning transmission electron microscopy (STEM), and ADT measurements were performed using a transmission electron microscope equipped with a field emission gun (Philips TECNAI F30 S-TWIN, accelerating voltage: 300 kV). HRTEM images and ED patterns were recorded with a CCD camera (Gatan US4000, 4k x 4k pixels). STEM images were recorded using a high-angle annular dark-field (HAADF) detector (Fischione). ED patterns were acquired with an automated acquisition module developed for FEI microscopes [13]. The ED patterns were hardware-binned by 2, resulting in 2k × 2k images. For ADT measurement, a dual-axis tomography holder (Fischione Model 2040) with a tilt range of ± 70° was used. The position for the data acquisition on the specimen was tracked in microprobe STEM mode with a small condenser aperture of 10 μm and a large spot size (gun lens 8, spot size 8) to minimize the electron dose on the sample. The beam size was set to about 75 nm in diameter. The tomographic ED acquisition was coupled with precession electron diffraction (PED) with 1° precession angle [18,19], using a dedicated unit (NanoMEGAS DigStar). A series of ED patterns were sequentially tilted with a fixed step of 1° and recorded with the exposure time of 3 seconds.

2.3. Other measurements

A powder X-ray diffractometer (BrukerAXS D8-Advance) was operated at 40 kV and 50 mA (λ = Cu Kα_1 provided by a Ge(111) primary monochromator) for obtaining accurate XRD data. The diffractometer is equipped with a modified Debye-Scherrer geometry, 1D position-sensitive detector (BrukerAXS VÅNTEC-1), and a Soller-slit with a 1.0° angler aperture. Thermogravimetric and differential thermal analysis (TG-DTA) was conducted under atmospheric conditions at the heating rate of 10 K·min^{-1} using a Bruker TG-DTA 2000SA apparatus. The Ar gas adsorption isotherm at 87 K was collected with a Bel Japan Belsorp max instrument. The adsorption measurement was conducted after the pretreatment at 473 K under vacuum for more than 2 h, and the equilibrium time for each measuring pressure was 300 s. The scanning electron microscopy (SEM) images were taken using a field emission-type microscope (Hitachi S-4800) at a low accelerating voltage of 1.0 kV and a working distance of 2 mm. Elemental analysis was carried out by using an energy dispersive X-ray spectrometry system (EDS) (BrukerAXS Quantax 200) with XFlash®6 detector, which was equipped on the above-mentioned FE-SEM operated at 20.0 kV, and a simultaneous inductively coupled plasma atomic emission spectrometer (ICP-AES) (Shimadzu ICPE-9820). The organic content of the materials was analyzed by a Yanaco MT-6 CHN Coder.

Local structures around H, Li, C, and Si atoms of as-synthesized THK-2 were investigated by the solid-state magic-angle-spinning (MAS) NMR experiments. ^{1}H MAS, ^{29}Si dipolar decoupled (DD) MAS, {^{1}H}$\rightarrow$^{29}Si cross-polarization (CP) MAS, and {^{1}H}$\rightarrow$^{13}C CP/MAS NMR spectra were recorded on a Bruker AVANCE III 400WB at 400.1 MHz for ^{1}H, at 79.5 MHz for ^{29}Si, and at 100.6 MHz for ^{13}C. In addition, the ^{7}Li MAS NMR spectrum was also collected at 155.5 MHz. A zirconia rotor with an inner diameter of 4 mm was used, and its spun rate was 6 kHz for ^{13}C and ^{29}Si and 14 kHz for ^{1}H and ^{7}Li. Each spectrum was accumulated

with the following conditions; a pulse length of 3.5 μs, recycle delay of 4 s for ^{1}H MAS, a pulse length of 5.24 μs (π/2 pulse), recycle delay of 60 s for ^{29}Si DDMAS, a contact time of 4 ms, recycle delay of 4 s for {^{1}H}→^{29}Si CP/MAS, a contact time of 4 ms, recycle delay of 4 s for {^{1}H}→^{13}C CP/MAS, and pulse length of 2 μs, recycle delay of 5 s for ^{7}Li MAS. Tetramethylsilane for ^{1}H and ^{29}Si, glycine for ^{13}C, and 1.0 M LiCl aqueous solution for ^{7}Li were used as chemical shift references.

2.4. Structure analysis

The ADT3D software [14] was used for the 3D ED data analysis, yielding unit-cell parameters, determining the space group, as well as extracting reflection intensities. Lattice constants and space groups were determined by the merged ED patterns acquired by ADT measurement. The initial structure model was obtained from direct methods implemented in Sir2014 [20] using ADT data based on the reflection intensities extracted from 3D ED data by assuming kinematic scattering conditions $I_{obs} \approx |F_{\mathrm{hkl}}|^2$.

Subsequently, the structure refinement using powder XRD data took place based on the obtained initial model. All intensity data in a whole powder pattern were analyzed by applying the Rietveld method using the RIETAN-FP program package [21]. In the early stage of refinement, we imposed restraints upon all the bond lengths l(Si–O) and l(Zn–O): l(Si–O) = 0.16±0.002 nm and l(Zn–O) = 0.18±0.04 nm, respectively, and the bond angles ϕ(O–Si–O) and ϕ(O–Zn–O): ϕ(O–Zn–O) = 109.47±3.0° and ϕ(O–Si–O) = 109.47±10.0°, respectively. Table 1 summarizes the experimental conditions and detailed crystallographic information (such as lattice parameters and R factors) for the samples. Besides, the disordered atomic arrangements of guest molecules taken up in the framework of the nanoporous material were estimated by

electron density distribution determined by the maximum entropy method (MEM) [22] using a program Dysnomia [23]. In order to simplify the structure refinement, hydrogen atoms in adsorbed water molecules were omitted, and a virtual atom (WO) was introduced; WO has the X-ray scattering amplitude corresponding to the summation of those of one O and two H atoms. Obtained structure models and electron density distributions were visualized utilizing the program VESTA3 [24]. Further detailed refinement conditions are described elsewhere.

3. Results and Discussion

3.1. Physicochemical properties

Crystallites of as-synthesized THK-2 have a rod-like morphology with a high aspect ratio of ca. 50~100 nm diameter × 0.5~1.5 μm length and are randomly aggregated (Figure 1). The EDS elemental analysis for as-synthesized THK-2 revealed C, O, Si, K, and Zn atoms, and average Si/Zn, and Si/K ratios were 10.2 and 23.0, respectively. The K atom distribution was somewhat inhomogeneous in the crystallite, whereas that of Zn atom was homogeneous. The EDS analysis of cal-THK-2 revealed that the K atom was hardly detected and that the Zn content decreased considerably (Si/Zn = 15.5). As described below, THK-2 samples contain impurities such as **MTW**-type zeolite and amorphous silica. Therefore, the ICP-AES cannot show the elemental composition only of THK-2. However, provided that Li and Zn are involved practically only in THK-2 after acetic acid-washing, ICP-AES estimates the Li/Zn ratios of as-synthesized and calcined THK-2 samples at 0.17 and 0.22, respectively.

Figure 2 shows the XRD patterns of THK-2 samples in the 2θ range from 3° to 50°. In the as-synthesized THK-2 sample, the **MTW**-type zeolite phase was identified (Figure 2(a)). Although a number of samples were synthesized under various conditions (Zn/Si, Li/Si, and

H_2O/Si ratios of mother gels or the temperature and time of hydrothermal treatment), the **MTW** phase and amorphous products were involved as impurities in all those samples. Also, as-synthesized sample without acetic acid washing showed strong diffraction peaks, which cannot be assigned, in the PXRD pattern (Figure S1). The crystallinity of cal-THK-2 was somewhat better than that of the as-synthesized sample, although the MTW phase remained. This fact is one of the reasons why cal-THK-2 was used for the following ADT structure determination.

TG-DTA measurement of as-synthesized THK-2 estimated that the amounts of occluded water and HMI molecule were 4.2 wt% and 4.3 wt%, respectively (Figure S2). These values were close to those calculated from CHN elemental analysis, 3.9 wt%, and 3.5 wt%. The structure of THK-2 was maintained up to the temperature of 950 K. An exothermic peak due to the structural collapse was observed at 960 K.

In the ^{1}H NMR spectrum of the as-synthesized sample (Figure 3(a)), a strong peak attributed to HMI molecule was observed at 2.94 ppm. Three small peaks at 0.65, 1.23, and 1.42 ppm could be attributed to silanol species (terminal or vicinal silanols). A broad resonance peak at 10.7 ppm can be assigned to the strong hydrogen bond of O–H···O. The O–O bond distance is estimated at 0.268 nm by using the Eckert equation [25]. This strong hydrogen bond suggests that the formation of local structures, such as silanol nests, at a defect region in the framework (see below). Similar strong hydrogen bonds have been found on the surface of some layered silicates where terminating silanol-siloxane species interact [26]. In the ^{13}C CP/MAS spectrum, two resonance peaks were observed, indicating that the HMI molecule is accommodated into the micropore of THK-2 without structural collapse (Figure 3(b)).

The ^{7}Li MAS NMR spectrum (Figure 3(c)) showed a doublet resonance peak around 0 ppm, suggesting that a local symmetry of Li^{+} ion would be high. A similar phenomenon has been

reported in lithosilicates RUB-23 [27] and RUB-29 [28], known as zeolitic analog compounds, including LiO_4 tetrahedra in the framework. Although Li^+ ion would be easily removed by strong acid treatment, a similar spectrum was observed in the cal-THK-2 sample treated with 1mM HCl aqueous solution (Figure S3). Therefore, it is proposed that Li^+ ions are somewhat stabilized by being trapped in a highly symmetric coordination environment. We speculate that the Li^+ ion was positioned to form a tetrahedral configuration by accident in the framework. Probably, a small amount of Li^+ ions partially occupies the same position as the Zn atom in as-synthesized THK-2 (please note that Li/Zn ratio of as-synthesized THK-2 is as low as 0.17, as described above).

In the ^{29}Si MAS NMR spectra, several resonance peaks showed a complex local structure of THK-2. In these spectra, resonance signals derived from the MTW phase or amorphous phase were overlapped. Therefore, we will limit our qualitative discussions of the attribution of local structures. Two or three resonance peaks in –108 ~ –114 ppm have been assigned to $Q^4(\underline{Si}(OSi)_4)$ local structure. A resonance peak around –103 ppm observed in the DDMAS spectrum (Figure 4(a)) was comparatively enhanced in the CP/MAS spectrum (Figure 4(b)). Then, this peak is attributed to $Q^3((SiO)_3\underline{Si}–OH)$ local environment. Also, the strongest peak was newly observed at –103.9 ppm in the CP/MAS spectrum. This phenomenon is generally due to the presence of silanol groups that actively interact with small molecules involving hydrogen atoms, and this applies to H_2O and HMI molecules. In such Si nuclei with many protons nearby, the signal intensity is usually increased significantly in CP/MAS measurement. Two resonance peaks at further downfield (–94 ppm and –96 ppm) are generally attributed to Q^3 local environment, but in this case, they should be assigned to $Q^4((SiO)_3\underline{Si}(OZn))$ units, similar to what had been observed near –93 ppm in the zincosilicate VPI-7 [29].

The Ar adsorption measurement of cal-THK-2 shows an isotherm close to Type I (BET-type defined by IUPAC [30]) isotherm curve (Figure 5). The adsorption volume was increased monotonically with increasing P/P_0 (>0.05), suggesting the presence of void space in aggregates, as seen in Figure 2. The specific surface area was estimated at 240.6 m^2/g. The NLDFT (Non-Localized Density Functional Theory) [31] analysis using the cylinder pore kernel model revealed that the nanopore diameter and its adsorption volume was 0.65 nm and 0.122 ml/g, respectively. The estimated pore diameter is almost compatible with an effective diameter of the 12-ring straight channel calculated from the structural model.

3.2. Framework structure of THK-2

Two different crystal morphologies, nearly isotropic particles, and long needles were observed from the STEM and TEM images (Figure S4, Figure S5). Therefore, ADT measurements were performed on single crystals of each morphology. In the reconstructions of 3D ADT data (Figure 6, Figure S6, Figure S7), the needle-like crystals show a primitive orthorhombic lattice confirming them as a new phase (THK-2), while the other crystals yielded a *C*-centred monoclinic lattice of a known zeolite MTW (Table 1). For the needle-like crystals of THK-2, the violation of the reflection conditions ($h = 2n + 1$ systematically absent in the $h0l$ plane) was not clearly visible in the diffraction data of the crystal Cry1 (Figure 6(e)) but obvious in the reconstructed ADT data of another crystal Cry2 (Figure S6). By combining the observed information from the three main planes of both Cry1 and Cry2 crystals, the reflection conditions can be concluded as follows: $l = 2n$ for $0kl$; $l = 2n$ for $h0l$ plane; $h + k = 2n$ for $hk0$ plane, leading to the extinction rule with the only possible space group *Pccn* (No. 56). The obtained lattice is almost identical to the hexagonal lattice ($a/b = 1.74 \approx 1.732$), confirming the intrinsic difficulty

for solving the structure of THK-2 only by powder XRD data due to the considerable overlap of the first several peaks.

Based on ADT reflection intensities obtained from Cry1, the ab initio structure solution of THK-2 using the direct method converged with a final residual of R = 0.17. A well-resolved Fourier potential map overlaid by a meaningful framework of all atoms was finally obtained (Figure 7(a)). Four strongest maxima (from 1.34 and 1.09 $e^{-}/Å^3$) are corresponding to Si atoms. The following maxima from 0.80 to 0.50 $e^{-}/Å^3$ are consistent with O atoms. Besides, one T site located at 8e site (0.249, 0.653, 0.528) having an average T–O distance (0.178 nm), which is much larger than that of Si–O (0.162 nm), was found on a maximum of 0.66 $e^{-}/Å^3$ comparable to the value of an O atom. We assumed that this T site would be partially occupied Zn atom (disorder distribution) (Figure 7(b) and (c)). The Zn site arrangement can be described as a chain of edge-sharing distorted [ZnO_4]-tetrahedra along the *c*-axis. However, considering the scattering power of Zn atoms, the Zn site population is considerably low (see Section 3.3), and the chain of shared edge tetrahedra should not be formed actually. A 12-ring straight channel is formed along the *c*-axis, and the shape of the channel was an elliptic cylinder with a diameter of ca. 0.71 nm × 0.60 nm. The cylinder diameter coincided with the pore size of 0.65 nm determined by the Ar gas adsorption experiment. The framework topology realized in THK-2 has many similarities to that of the MTW type structure; that is, both frameworks have a 12-ring straight channel and consist of 4-, 5- and 6-rings. Also, the *jbw* (10T) composite building unit [32] is included in both structures.

3.3. Structure refinement

To complete the structure analysis, the initial model of cal-THK-2 obtained from the direct

methods based on ADT data was refined using the Rietveld method implemented in the program package RIETAN-FP (Figure 8). The above described 8e site with long T–O distance was assigned to the Zn atom, and its occupancy parameter *g*(Zn) was so small as ca. 0.26. Therefore, two adjacent Zn sites with too short Zn-Zn distance of 0.253 nm is not occupied simultaneously. A positional disorder model explains the Zn atom distribution on the 8e site. From this result, a large number of silanol nests will be present around the defect site of the Zn atom, and the sites O2 and O5 around the defect position of Zn atom should be considered as –OH groups. In most Zn atom deficient regions, columnar spaces where silanols are formed along the *c*-axis. In other words, we can interpret that Zn atoms are trapped in the column space filled with silanols. This consideration is supported by the presence of a Q^3 signal in ^{29}Si NMR spectra and a downfield signal in the ^{1}H NMR spectrum. Due to many vacancies, we expect that other transition metal ions will be substituted at the Zn site.

In the 12-ring straight channel, small peaks in a MEM electron density map was detected, which can be attributed to an adsorbed H_2O molecule (sites WO1 and WO2). Those occupancy parameters, *g*, converged to 0.32(3) for WO1, and 0.17(3). Furthermore, two small peaks attributed to additional H_2O molecules were detected around the center of 5-ring; site WO3 is located at 8*e* site (0.444, 0.727, 0.462) with *g*(WO3) ≈ 0.44. The interatomic distance between site WO3 and adjacent atom was 1.99(6) Å for *l*(WO3–O5) and 2.24(5) Å for *l*(WO3–Si2), which is somewhat short. This is probably because most site O5 is an –OH group, and water molecules are weakly bonded to site O5.

The Li atom position could not be determined uniquely. It is likely that Li might partially occupy the Zn site because the ^{7}Li-NMR measurement suggested the presence of the Li atom's tetrahedral coordination. If Li^+ and Zn^{2+} ions are located at the 8e site (non-Si tetrahedral site),

a part of –OH groups of sites O2 or O5 are reinterpreted $–O^-$ in order to keep a local charge balance. Based on all the experimental results above, the estimated structural composition was denoted as $|(H_2O)_{7.6}|[Li_{0.5}Zn_{2.1}Si_{32}O_{60.7}(OH)_{11.3}]$. This composition allows the charge balance in the unit cell to be kept neutral. The MTW phase content was estimated to be 18.3 wt% from the refined scale factors of the two-phase Rietveld analysis.

In as-synthesized THK-2, a complicated arrangement of HMI molecule was revealed by the structure refinement (Figure S8). As a first step, the HMI molecule distribution was determined utilizing the direct space method using a program FOX [33]. In this analysis, bond lengths and bond angles among C, N, and H atoms were restrained to keep molecular geometry reasonable. The positions of the HMI molecule were fixed at the positions obtained by the direct space method during structure refinement because the resolution of the PXRD data was low, and the accuracy of the analysis was insufficient. The occupancy of HMI was fixed to 0.108 calculated from the result of CHN analysis.

Then, the HMI molecule was found inside the 12-ring straight channel, and the center position of the molecule was somewhat displaced from its center axis (Figure S8(a), (b)). The HMI ring plane is roughly parallel to the *a*-*b* plane (Figure S8(c)). The refined *g*(Zn) value was 0.39, indicating that Zn content was about 30% higher than that of the calcined sample. Zn atoms may have been eliminated by HCl treatment. By the MEM analysis, one H_2O site was detected beside the HMI molecule, and its content was estimated at 4.9 wt%. This finding was consistent with the result of TG-DTA analysis. The position of Li^+ ion, as well as the calcined samples, is not determined so far, and the position of K^+ ion could also not be specified because the K content was minimal. Since K^+ ions were not present in the calcined sample, the distribution of K^+ ions within the THK-2 framework would be intrinsically unstable. From the

above consideration, the presence of K^+ ion was omitted. The structural composition was estimated to be $|(H_2O)_{6.7}(C_6H_{13}N)_{0.9}|[Li_{0.5}Zn_{3.1}Si_{32}O_{62.7}(OH)_{9.3}]$. Refined lattice constants were slightly larger than those of cal-THK-2 (Table 2). This fact suggests that the framework of THK-2 is expanded by the presence of a guest molecule in the channel. The total amount of MTW phase was estimated at 22.8 wt%, which is somewhat higher than that of cal-THK-2. This finding suggests that the fibrous crystal of THK-2 collapsed by calcination and transformed into an amorphous phase. Calculated Si/Zn values are 15.2 for cal-THK-2 and 10.3 for as-synthesized THK-2, which are in good agreement with those determined by EDX analysis for some selected THK-2 crystallites. Finally, the Rietveld analysis for cal-THK-2 and as-synthesized THK-2 yielded the final *R* factors of R_F = 1.0% (Figure 9) using 2409 F_o's and R_F = 0.2% (Figure S9) using 2427 F_o's, respectively.

Conclusion

The crystal structure of a new nanoporous zincosilicate THK-2, obtained using Li^+, K^+, and HMI as structure directors during the hydrothermal reaction, was solved employing the robust combination analysis of ADT and powder XRD techniques from disordered crystals in the nano-size regime. THK-2 has a 12-ring straight channel and consists of 4-, 5-, 6-rings, and the *jbw* (10T) composite building unit, as is the case in MTW-type zeolite that is observed as a byproduct. In the as-synthesized sample, HMI molecules were found in the 12-ring straight channel disorderly.

The local environment around the Zn atom in THK-2 is four-coordinated $[ZnO_4]$-tetrahedra, whereas the distribution of Zn atoms is disordered, and the site occupancy was as low as 0.26 in the calcined form. Hence a large number of silanols are present around the Zn atom residing

in structural vacancies. This consideration is supported by the presence of a strong hydrogen bond observed by ^{1}H MAS NMR measurement. The presence of the four-coordinated Li atom was presumed by ^{7}Li MAS NMR measurement. Since Li^{+} ions remain even after the treatment with acetic acid or HCl, probably Li atoms partially and stably occupy the same sites as Zn atoms, although the structure analysis could not determine Li atom position. This means that THK-2 is considered not as a lithium-type zincosilicate but as a lithozincosilicate.

Conflicts of interest

There are no conflicts to declare.

Acknowledgements

Y.S. gratefully acknowledges PRESTO, Japan Science and Technology Agency (JST) for the financial support. H.Z. gratefully acknowledges the Carl Zeiss Stiftung for the financial support.

Footnote

† Electronic supplementary information (ESI) available: Experimental details including synthetic, spectroscopic and crystallographic.

Notes and References

1. T. Tatsumi, "Metal-Substituted Zeolites as Heterogeneous Oxidation Catalysts" in *Modern Heterogeneous Oxidation Catalysis: Design, Reactions and Characterization*, ed. N. Mizuno, Wiley-VCH Verlag GmbH & Co. KGaA, 2009, ch. 4, pp. 125–155.
2. M. Shamzhy, M. Opanasenko, P. Concepciónb and A. Martínez, *Chem. Soc. Rev.*, 2019, **48**, 1095–1149.
3. T. Mole, J. R. Anderson and G. Creer, *Appl*. *Catal*., 1985, **17**, 141–154.
4. M. S. Scurrell, *Appl*. *Catal*., 1988, **41**, 8–98.
5. P. McAnespie, A. Dyer and B. J. Mehta, *U.S. Patent* 4,329,328, 1982.
6. R. W. Broach, N. Greenlay, P. Jakubszak, L. M.Knight, S. R. Miller, J. P. S. Mowat, J. Stanczyk and G. J. Lewis, *Micropor. Mesopor. Mater*., 2014, **189**, 49–63.
7. N. Rajic, N. Z. Logar and V. Kaucic, *Zeolites*, 1995, **15**, 672–678.
8. C. Röhrig and H. Gies, *Angew*. *Chem*. *Int*. *Ed*., 1995, **34**, 63–65.
9. X. Bu, P. Feng and G. D. Stucky, *Science*, 1997, **278**, 2080–2085.
10. L. B. McCusker, R. W. Grosse-Kunstleve, Ch. Baerlocher, M. Yoshikawa and M. E. Davis, *Microporous Mater*., 1996, **6**, 295–309.
11. M. J. Annen, M. E. Davis, J. B. Higgins and J. L. Schlenker, *Chem*. *Commun*., **1991**, 1175–1176.
12. B. Marler, J. Patarin and L. Sierra, *Microporous Mater*., 1995, **5**, 151–159.
13. U. Kolb, T. Gorelik, C. Kübel, M. T. Otten and D. Hubert, *Ultramicroscopy*, 2007, **107**, 507–513.
14. U. Kolb, T. Gorelik and M. T. Otten, *Ultramicroscopy*, 2008, **108**, 763–772.
15. U. Kolb, E. Mugnaioli and T. E. Gorelik, *Cryst*. *Res*. *Technol*., 2011, **46**, 542–554.
16. E. Mugnaioli and U. Kolb, *Micropor*. *Mesopor*. *Mater*., 2013, **166**, 93–101.

17. E. Mugnaioli and U. Kolb, *Micropor. Mesopor. Mater.*, 2014, **189** 107–114.

18. E. Mugnaioli and T. Gorelik , U. Kolb, *Ultramicroscopy*, 2009, **109**, 758–765.

19. R. Vincent and P. A. Midgley, *Ultramicroscopy*, 1994, **53**, 271–282.

20. M. C. Burla, R. Caliandro, B. Carrozzini, G. L. Cascarano, C. Cuocci, C. Giacovazzo, M. Mallamo, A. Mazzoneand and G. Polidori, *J. Appl. Cryst.*, 2015, **48**, 306–309.

21. F. Izumi and K. Momma, *Solid State Phenom.*, 2007, **130**, 15–20.

22. K. Knorr, F. Madler and R. J. Papoular, *Microporous Mesoporous Mater.*, 1998, **21**, 353–363.

23. K. Momma, T. Ikeda, A. A. Belik and F. Izumi, *Powder Diff.*, 2013, **28**, 184–193.

24. K. Momma and F. Izumi, *J. Appl. Crystallogr.*, 2011, **44**, 1272–1276.

25. H. Eckert, J. P. Yesinowski, L. A. Silver and E. M. Stolper, *J. Phys. Chem.*, 1988, **92**, 2055–2064.

26. C. Gardiennet and P. Tekely, *J. Phys. Chem. B*, 2002, **106**, 8928–8936.

27. S. -H. Park, P. Daniels and H. Gies, *Microporous Mesoporous Mat.*, 2000, **37**, 129–143.

28. S. -H. Park, J. B. Parise, H. Gies, H. Liu, C. P. Grey and B. H. Toby, *J. Am. Chem. Soc.*, 2000, **122**, 11023–11024.

29. C. Röhrig, H. Gies and B. Marler, *Zeolite*, 1994, **14**, 498–503.

30. M. Thommes, K. Kaneko, A. V. Neimark, J. P. Olivier, F. Rodriguez-Reinoso, J. Rouquerol and K. S. W. Sing, *Pure Appl. Chem*. 2015, **87**, 1051–1069.

31. P. Tarazona, U. Marini Bettolo Marconi and R. Evans, *Mol. Phys.*, 1987, **60**, 573–595.

32. Ch. Baerlocher, L.B. McCusker and D.H. Olson, *Atlas of Zeolite Framework Types*, 6th revised edition, Elsevier, Amsterdam, p375, 2007.

33. V. Favre-Nicolin and R. Cerny, *J. Appl. Cryst.*, 2002, **35**, 734–743.

Figure captions

Figure 1. SEM micrographs of as-synthesized THK-2 showing rod-like morphology.

Figure 2. PXRD patterns of (a) as-synthesized THK-2 and (b) cal-THK-2. Arrows indicate the reflection peaks attributed to MTW phase.

Figure 3. (a) ^{1}H, (b) ^{13}C CP/MAS, and (c) ^{7}Li MAS NMR spectra of as-synthesized THK-2.

Figure 4. (a) $\{^{1}H\}\rightarrow^{29}Si$ CP/MAS NMR and (b) ^{29}Si DDMAS NMR spectra of as-synthesized THK-2.

Figure 5. Ar adsorption isotherm at 87 K of cal-THK-2. Inset shows pore size distribution and cumulative pore volume.

Figure 6. (a-c) Reconstructed 3D reciprocal volume of THK-2 (Cry1) obtained from ADT data viewed down the three main directions. (d-f) 2D 0kl, h0l and hk0 slices cut from ADT dataset. The crystal size and morphology of Cry1 is shown as an insert in (d).

Figure 7. (a) A well-resolved Fourier potential map and extracted framework model viewed along (b) [001] and (c) [100] directions obtained by the ADT analysis.

Figure 8. Refined crystal structure model of cal-THK-2 viewed along (a) [001], (b) [010] and (c) [100] directions. Blue, red, yellow and green spheres indicate Si, O, Zn and H_2O positions, respectively. (d) Edge-sheared ZnO_4 chain (Yellow) is formed along [001] direction in framework, and (e) T–T connectivity composed of 4-, 5- and 6-rings forms a 12-ring straight channel viewed along [001] direction.

Figure 9. Observed, calculated and difference patterns, and background obtained by the Rietveld refinement for cal-THK-2.

Table 1. Crystallographic data from reconstructed electron diffraction volume and experimental details for structure solution of THK-2 in space group *Pccn*.

Crystallographic data of THK-2 and MTW obtained from ADT data		
Materials	THK-2	MTW
Crystal system	Orthorhombic	Monoclinic
Extinction symbol	*P c c n*	*C* 1 *c* 1
a / Å	24.70	25.09
b / Å	14.55	5.00
c / Å	4.99	24.15
α / °	90	90
β / °	90	108.1
γ / °	90	90
ADT experiments and structure solution details of THK-2		
Tilt range	–60 / +65	
Number of total reflections	3339	
Number of independent reflections	705	
Space group	*P c c n*	
Reflection coverage (%)	99	
Resolution (Å)	1.1	
R_{int}	0.113	
Overall U(Å^2)	0.047	
Residual *R* (SIR2014)	0.17	

Table 2. Obtained crystallographic information of THK-2 by Rietveld refinement.

Sample name	cal-THK-2	as-synthesized THK-2
Estimated structural composition	$\lvert(H_2O)_{7.5}\rvert$ $[Li_{0.5}Zn_{2.1}Si_{32}O_{60.7}(OH)_{11.3}]$	$\lvert(C_6H_{13}N)_{0.9}(H_2O)_{6.7}\rvert$ $[Li_{0.5}Zn_{3.1}Si_{32}O_{62.7}(OH)_{9.3}]$
Refined structural composition	$\lvert(H_2O)_{7.5}\rvert$ $[Zn_{2.1}Si_{32}O_{60.7}(OH)_{11.3}]$	$\lvert(C_6H_{13}N)_{0.9}(H_2O)_{6.7}\rvert$ $[Zn_{3.1}Si_{32}O_{62.7}(OH)_{9.3}]$
F_W	2321.4	2460.0
Space group	*Pccn* (No. 56, set. 2)	←
a / nm	2.48056(12)	2.50376(6)
b / nm	1.437761(7)	1.43869(4)
c / nm	0.503675(12)	0.505369(8)
Unit-cell volume, V / nm^3	1.79614(13)	1.82041(8)
Wavelength, λ / nm	0.1540593 (Cu Kα_1)	←
2θ range/°	4.0–100.1	←
Step size, 2θ / °	0.017368	←
Counting time per step / s	16333	←
Profile range in the unit of FWHM	12	←
FWHM / °	0.1685 (at 2θ = 20.971°)	0.224 (at 2θ = 20.934°)
Number of intensity data	5904	←
Number of contributing reflections	2409	←
Number of refined structural parameters	58	54
Number of background parameters	12	←
Number of nonlinear restraints	44	44
R_F (Rietveld)	0.010	0.002
R_{Bragg} (Rietveld)	0.010	0.003
R_{wp} (Rietveld)	0.031	0.020
R_p (Rietveld)	0.023	0.015
R_{exp} (Rietveld)	0.017	0.008
χ^2	1.8	2.4
R_F (MEM)	0.008	0.009
wR_F (MEM)	0.011	0.009

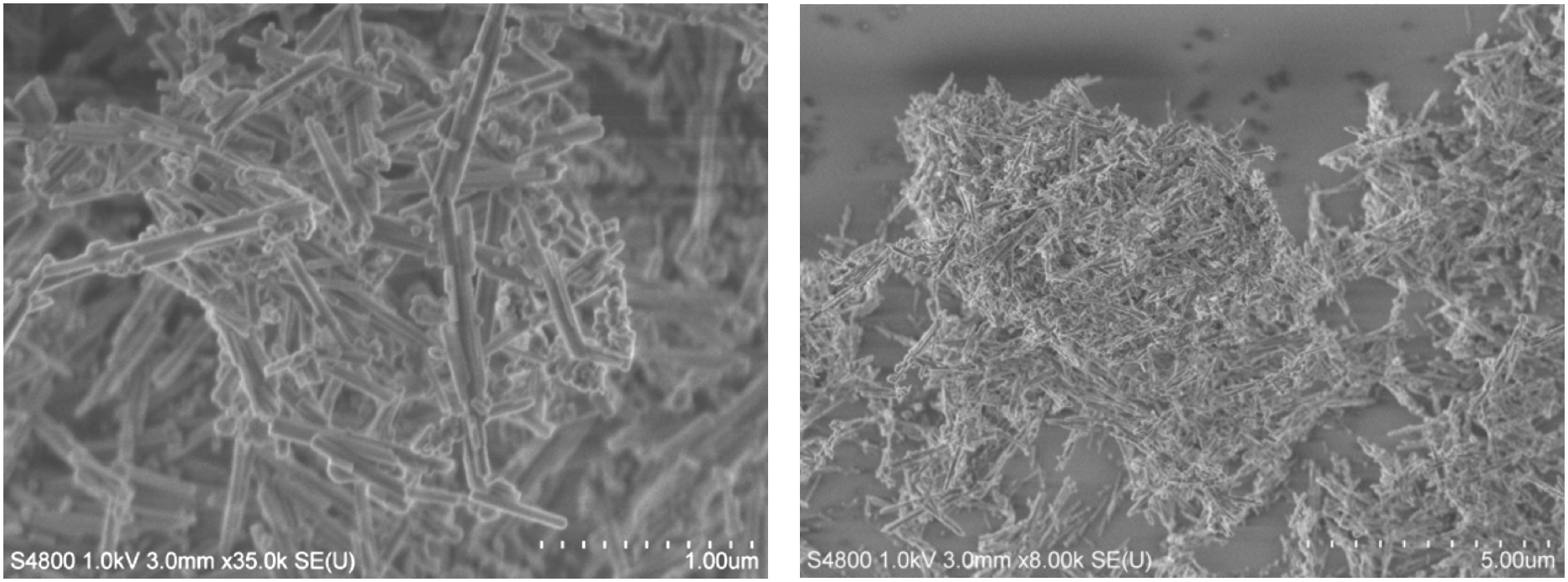

Figure 1. SEM micrographs of as-synthesized THK-2 showing rod-like morphology.

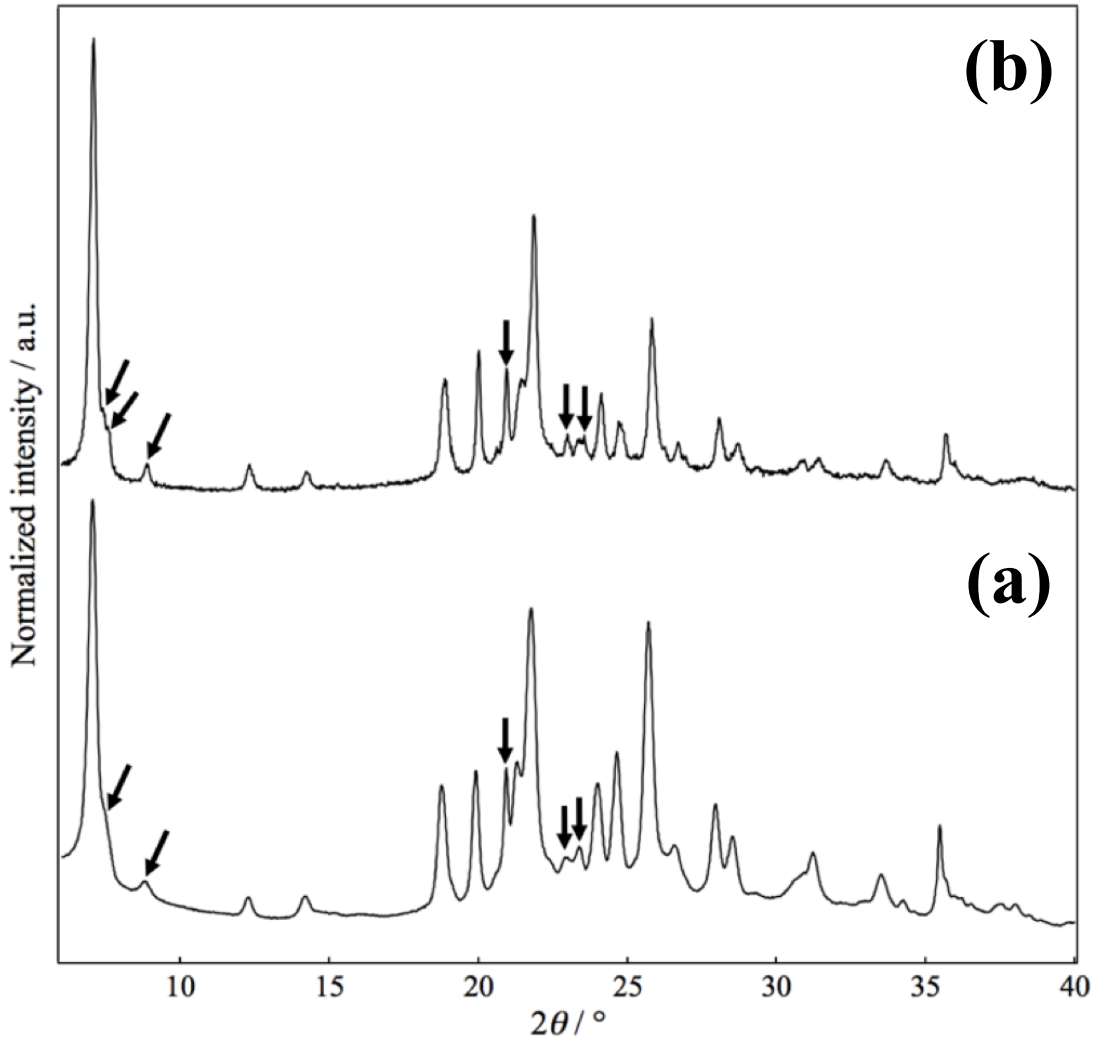

Figure 2. PXRD patterns of (a) as-synthesized THK-2 and (b) cal-THK-2. Arrows indicate the reflection peaks attributed to MTW-phase.

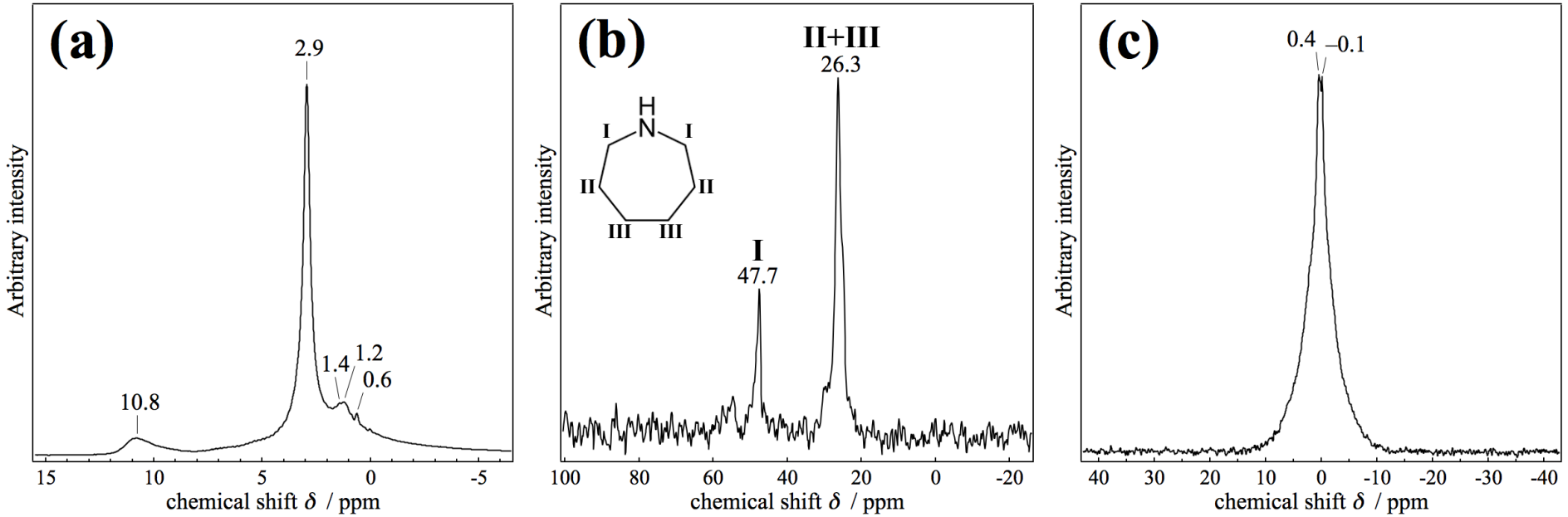

Figure 3. (a) ^{1}H, (b) ^{13}C CP/MAS, and (c) ^{7}Li MAS NMR spectra of as-synthesized THK-2.

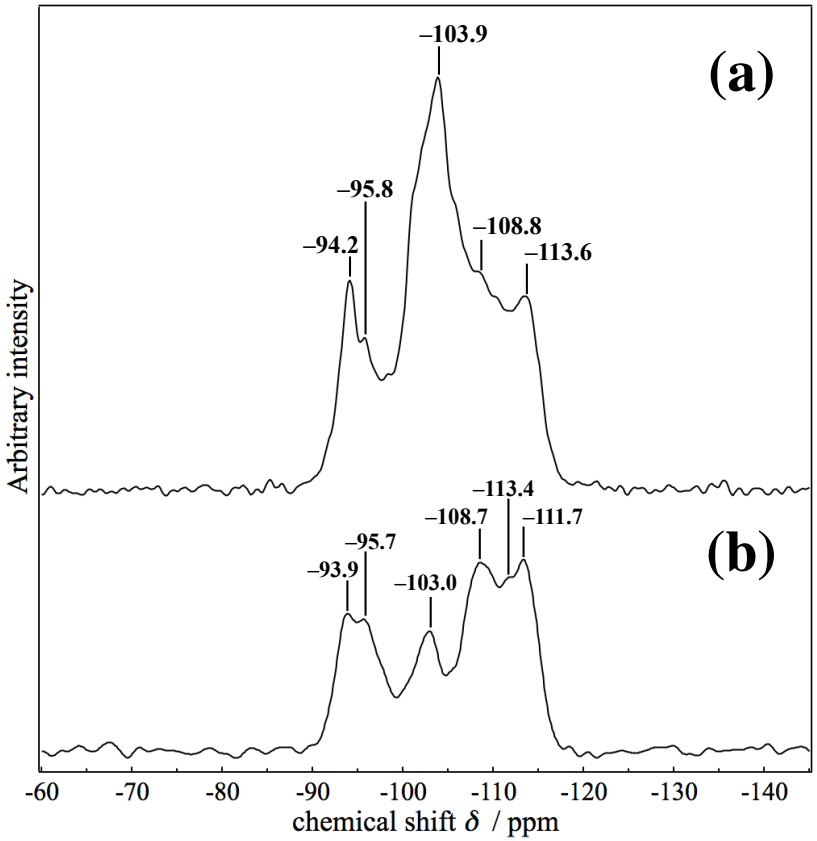

Figure 4. (a) $\{^{1}H\}\rightarrow^{29}Si$ CP/MAS NMR and (b) ^{29}Si DDMAS spectra of as-synthesized THK-2.

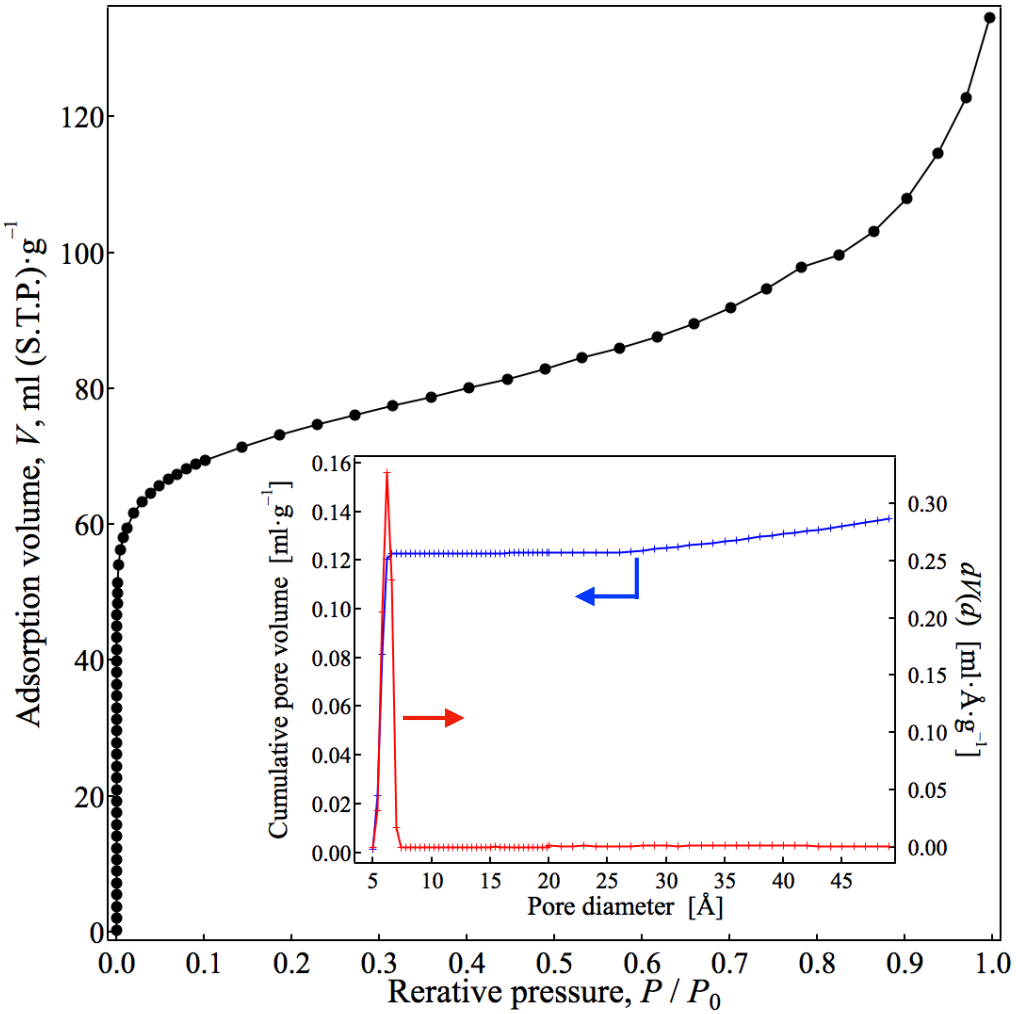

Figure 5. Ar adsorption isotherm at 87 K of cal-THK-2. Inset shows pore size distribution and cumulative pore volume.

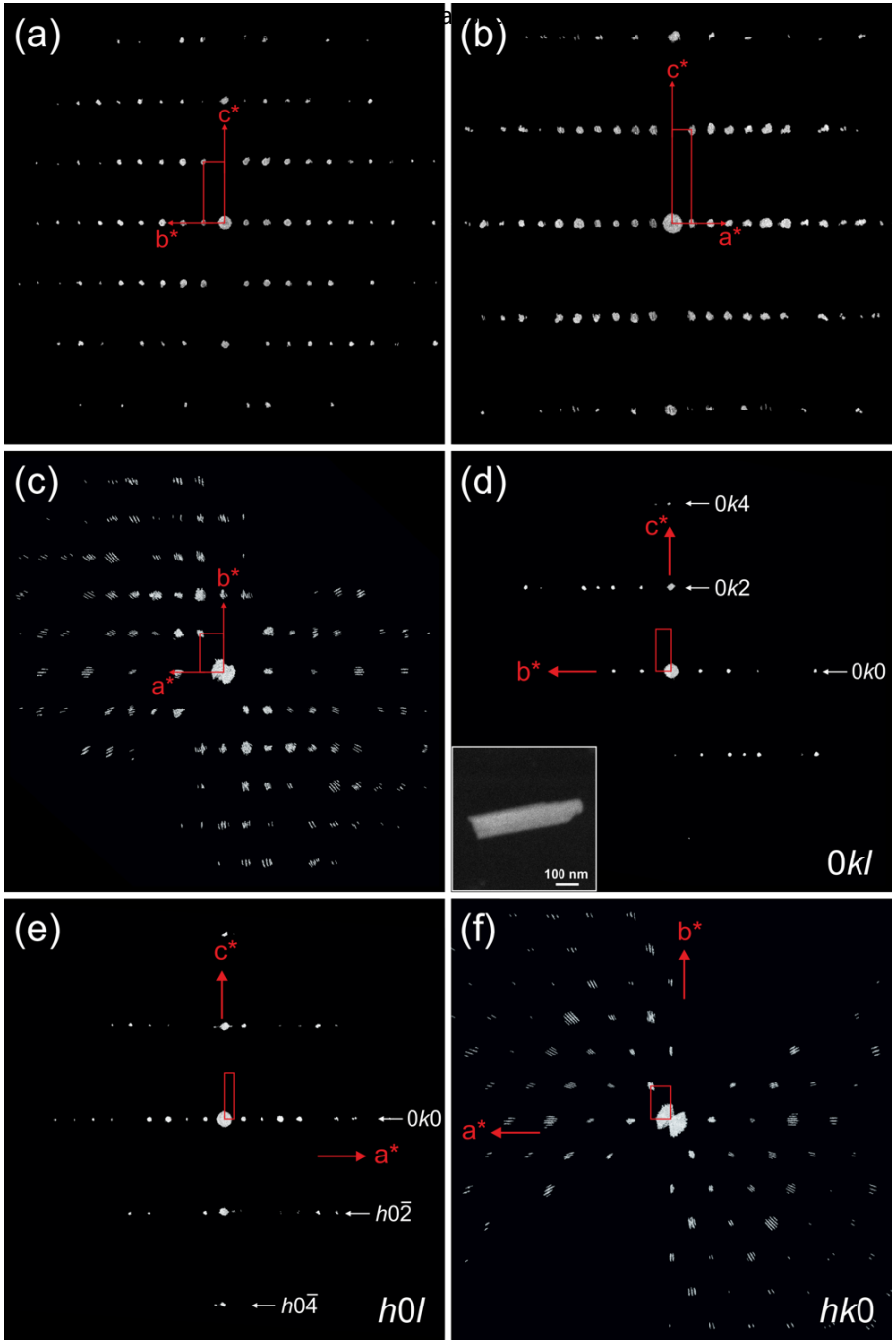

Figure 6. (a-c) Reconstructed 3D reciprocal volume of THK-2 (Cry1) obtained from ADT data viewed down the three main directions. (d-f) 2D 0*kl*, *h*0*l* and *hk*0 slices cut from ADT dataset. The crystal size and morphology of Cry1 is shown as an insert in (d).

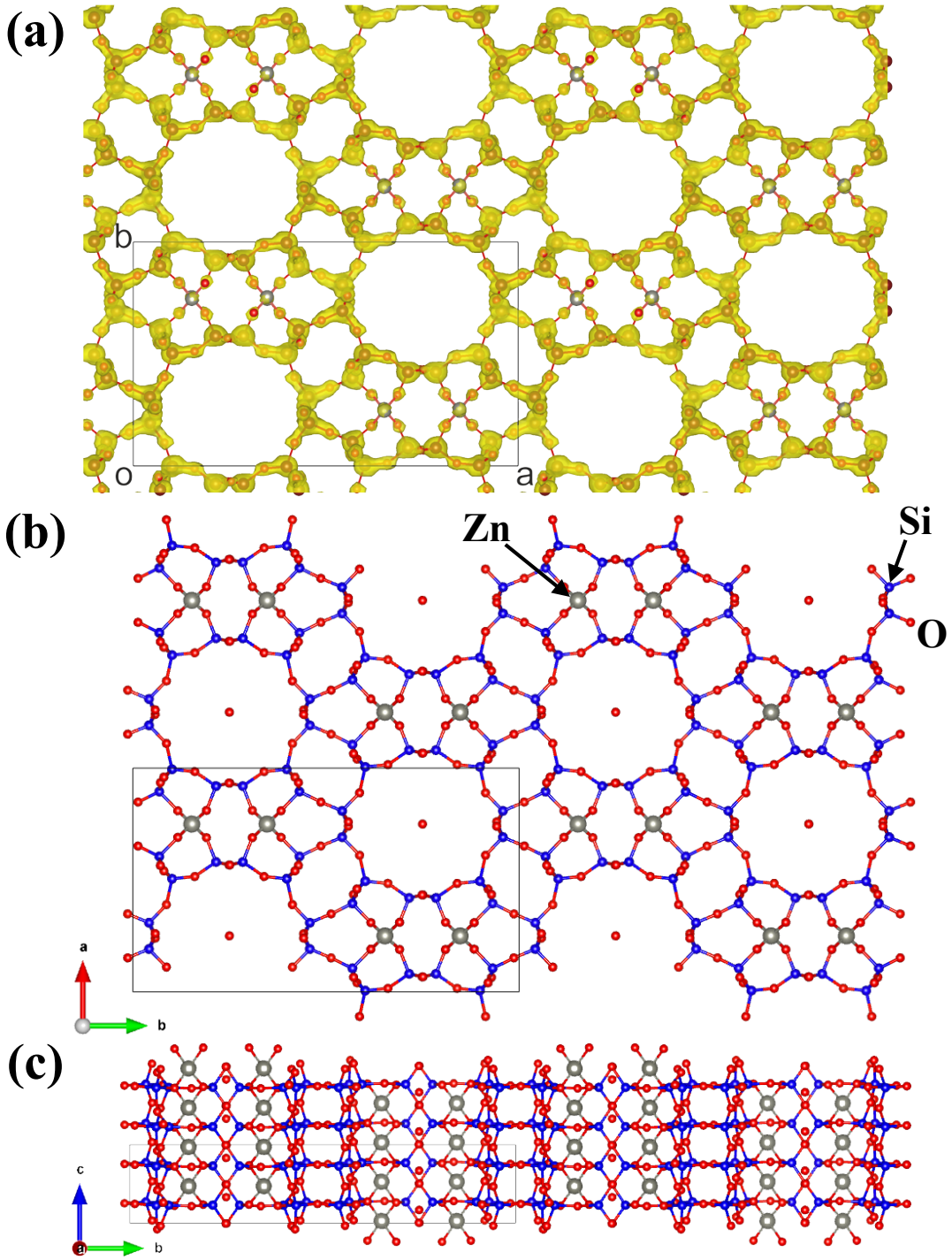

Figure 7. (a) A well-resolved Fourier potential map and extracted framework model viewed along (b) [001] and (c) [100] directions obtained by the ADT analysis.

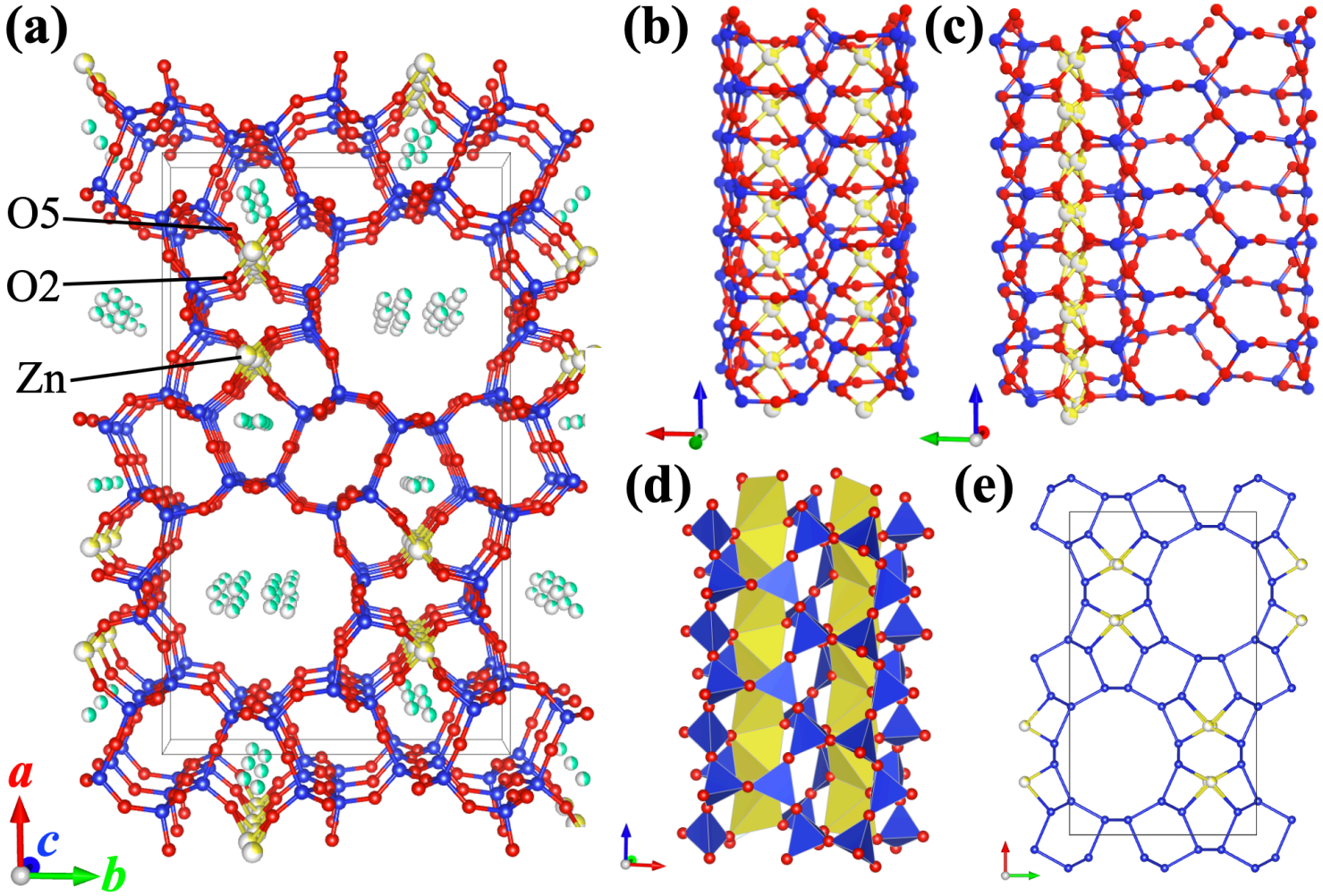

Figure 8. Refined crystal structure model of cal-THK-2 viewed along (a) [001], (b) [010] and (c) [100] directions. Blue, red, yellow and green spheres indicate Si, O, Zn and H_2O positions, respectively. (d) Edge-sheared ZnO_4 chain (Yellow) is formed along [001] direction in framework, and (e) T–T connectivity composed of 4-, 5- and 6-rings forms a 12-ring straight channel viewed along [001] direction.

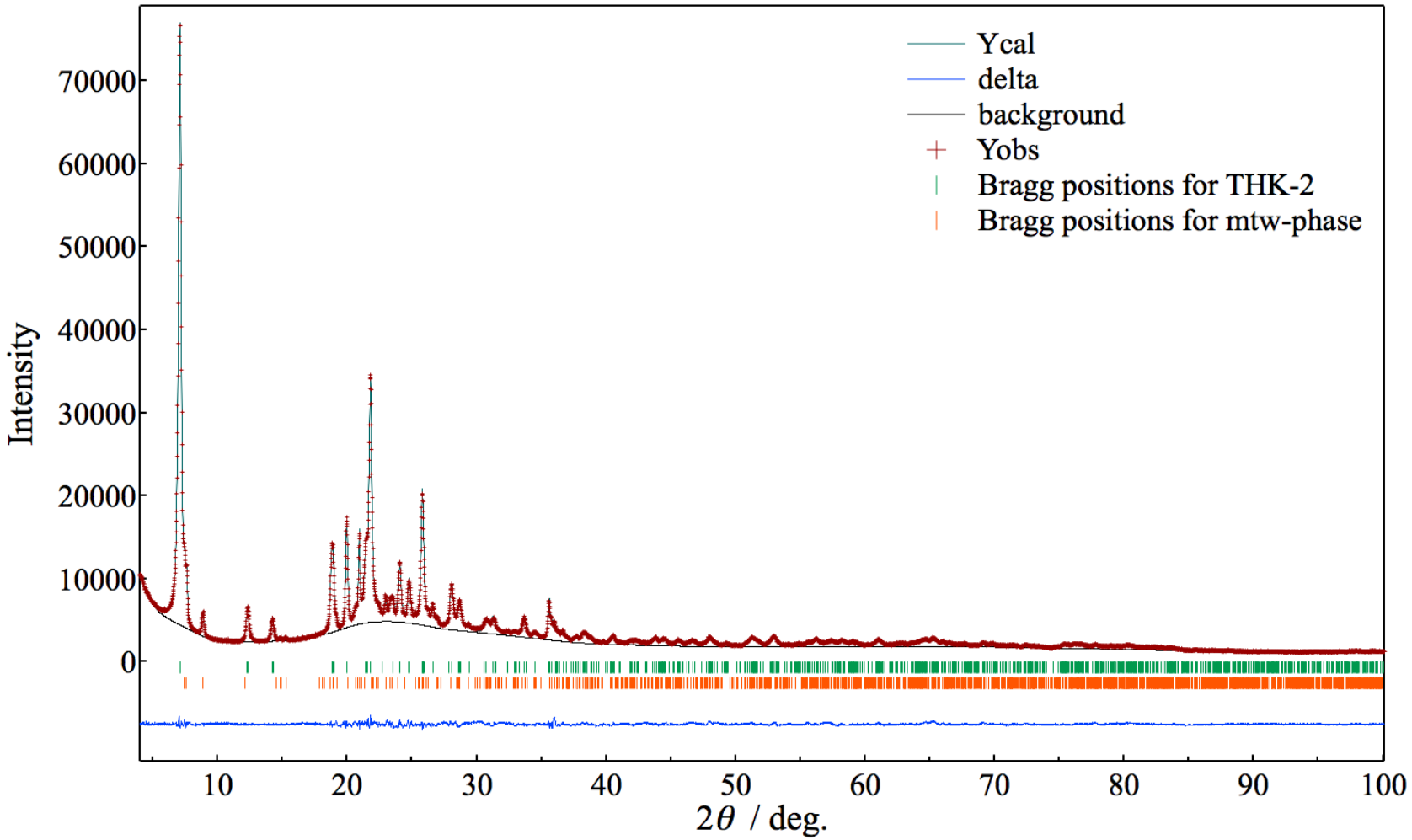

Figure 9. Observed, calculated and difference patterns, and background obtained by the Rietveld refinement for cal-THK-2.

Table of contents entry

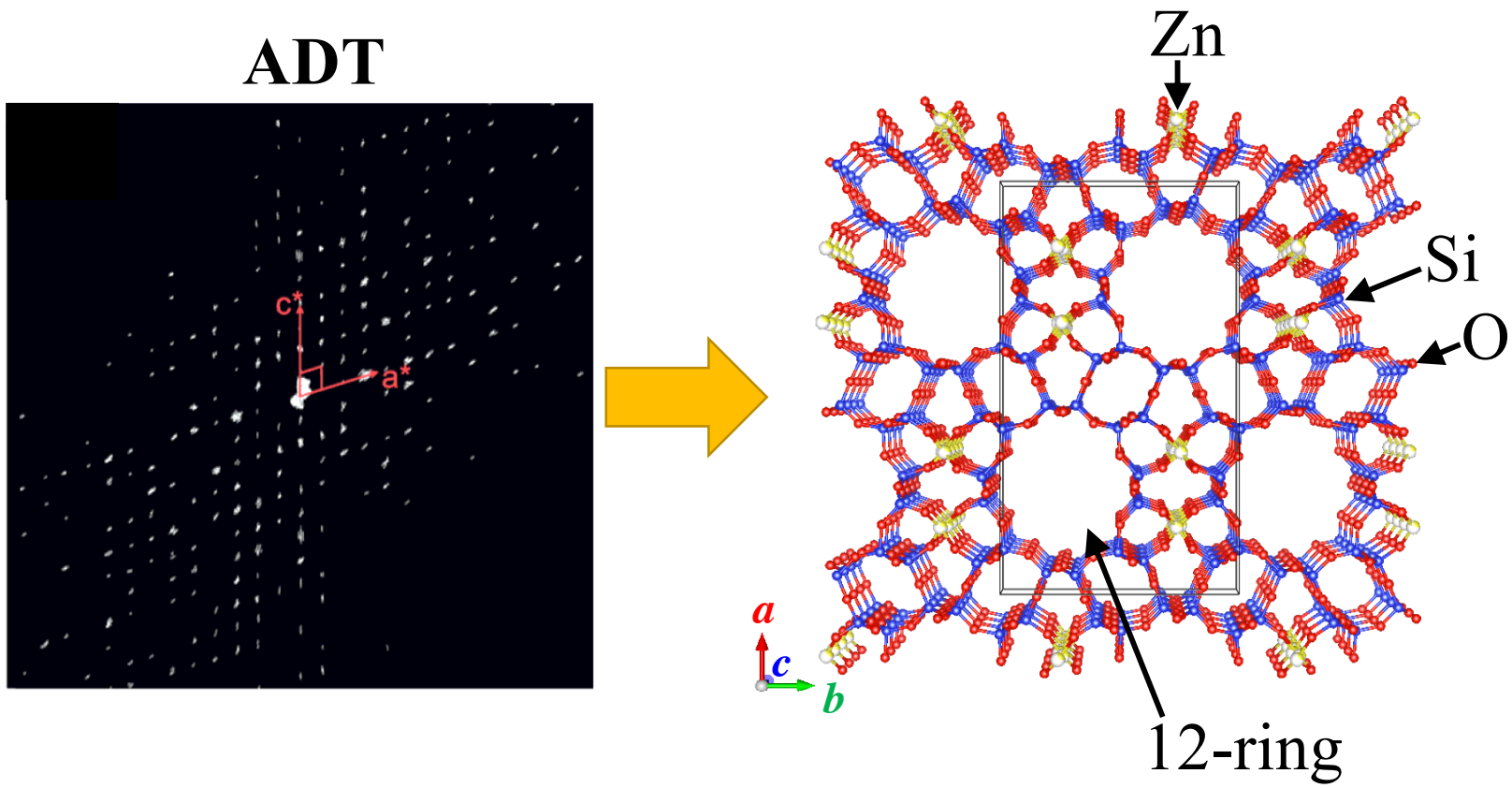

The crystal structure of new microporous zincosilicate THK-2 was elucidated by using the automated electron diffraction tomography (ADT) approach. The framework of THK-2 consists of 4-, 5-, 6-, and 12-ring and includes a distorted ZnO_4 with low occupancy.